


Super-Poissonian behavior of the Rosenzweig-Porter model in the nonergodic extended regimeRichard Berkovits *Department of Physics, Jack and Pearl Resnick Institute, Bar-Ilan University, Ramat-Gan 52900, Israel* (Received 8 July 2020; revised 8 October 2020; accepted 8 October 2020; published 22 October 2020)

The Rosenzweig-Porter model has seen a resurgence in interest as it exhibits a nonergodic extended phase between the ergodic extended metallic phase and the localized phase. Such a phase is relevant to many physical models from the Sachdev-Ye-Kitaev model in high-energy physics and quantum gravity to the interacting many-body localization in condensed-matter physics and quantum computing. This phase is characterized by fractal behavior of the wave functions and a postulated correlated miniband structure of the energy spectrum. Here we will seek evidence for the latter in the spectrum. Since this behavior is expected on intermediate energy scales, spectral rigidity or number variance is a natural way to tease it out. Nevertheless, due to the Thouless energy and ambiguities in the unfolding procedure, the results are inconclusive. On the other hand, by using the singular-value decomposition method, clear evidence for a super-Poissonian behavior in this regime emerges, consistent with a picture of correlated minibands.

DOI: [10.1103/PhysRevB.102.165140](https://doi.org/10.1103/PhysRevB.102.165140)

The Anderson metal-insulator transition continues to surprise even after six decades [1]. The canonical picture for a single-particle Anderson transition is the three-dimensional Anderson model, which shows a metal-insulator transition for a critical value of on-site disorder. For weak disorder the system is metallic, and the wave function is extended, while for stronger disorder the wave function is localized, and the system is insulating [2,3]. At the critical disorder the wave function is fractal [4]. The energy spectrum also reflects these phases. In the localized regime the level spacing distribution (corresponding to small energy scales and large times) follows the Poisson distribution, while for the extended regime it corresponds to the Wigner-Dyson (WD) distribution. [5–8]. Several forms of the level spacing were suggested at criticality [9–12]. For larger energy scales, the spectral rigidity or the variance of the number of levels in a given energy window is a useful indicator. For the localized phase the variance is equal to the average number of states in this window, while for the extended phase it is proportional to the logarithm of the average. At the critical point the variance is proportional to the average number of states, with a proportionality lower than 1 [13–15].

An additional energy scale relevant to disordered metals is the Thouless energy $E_T = g\Delta$ (where g is the dimensionless conductance and Δ is the average level spacing) [13]. While WD predictions hold up to an energy scale $E < E_T$, above which a nonuniversal behavior takes over. The physical origin of the Thouless energy is the onset of diffusive behavior.

There has been a recent surge of interest in the critical behavior of the transition. Part of this interest stems from the realization that for the many-body localization phenomenon the localized and extended regions may be separated by a critical regime [16–25]. An additional motivation pertains to the Sachdev-Ye-Kitaev (SYK) model, originally introduced in the study of spin liquids [26] and recently gaining relevance

to holographic dualities in string theory [27] and quantum gravity [28]. There is evidence the SYK model perturbed by a single-body term shows a critical region [29]. This model also shows a signature of the existence of a Thouless energy [30].

The generalized Rosenzweig-Porter (GRP) random matrix model [31,32] is considered the simplest model for which the localized and fully ergodic phases both exist, with a non-ergodic extended (NEE) phase separating them. Almost all evidence for the NEE comes from the study of the fractality of the wave functions [32–37]. In Ref. [38] some tantalizing clues for super-Poissonian behavior appeared in the n th level spacing distribution. Finding fingerprints of NEE in the energy spectrum is important for both theoretical and practical reasons. It is much easier numerically, as well as experimentally, to obtain the energies than to obtain wave functions for large systems. Here we examine two methods to garner such information: the venerable method of number variance [39] and singular-value decomposition (SVD) [40–42]. Both will be used to study very large GRP matrices on scales of thousands of eigenvalues. It turns out that although the number variance exhibits anomalies which could be attributed to NEE, it is nevertheless hard to separate them from the effects of the Thouless energy, finite size, and dependence on unfolding. On the other hand, SVD seems to provide strong evidence for an intermediate scale of energy, for which systems belonging to the NEE phase show super-Poissonian behavior of the spectra, similar to the random Cantor set behavior [17].

The GRP is defined by a random matrix H_{ij} , of size $N \times N$, where the diagonal terms are chosen from a certain distribution while the off-diagonal term is chosen from a distribution with a variance proportional to $N^{-\gamma}$. Specifically, we have chosen the diagonal H_{ii} from a box distribution with a range $-\sqrt{6}/2, \dots, \sqrt{6}/2$ ($\delta^2 \langle H_{ii} \rangle = 1/2$) and the off-diagonal $H_{i \neq j}$ from a box distribution between $-N^{-\gamma/2}/2$

and $N^{-\gamma/2}/2$ ($\langle \delta^2 H_{i \neq j} \rangle = N^{-\gamma}/12$), thus corresponding to $N^\gamma \langle H_{i \neq j}^2 \rangle / \langle H_{ii}^2 \rangle = 1/6$.

For GRP one expects a transition from localized to extended behavior at $\gamma = 2$ [32,38,43–48]. This transition is manifested in the energy spectrum of the system in a transition in the nearest neighbor level distribution between Poissonian behavior for $\gamma > 2$ to WD like repulsion at $\gamma < 2$. The finite-size scaling of this behavior is clearly seen by the ratio statistics, defined as

$$r_s = \langle \min(r_n, r_n^{-1}) \rangle, \quad r_n = \frac{E_n - E_{n-1}}{E_{n+1} - E_n}, \quad (1)$$

where E_n is the n th eigenvalue of the matrix and $\langle \dots \rangle$ is an average over different matrices and a range of eigenvalues. For the Poisson distribution one expects $r_s = 2 \ln(2) - 1 \sim 0.3863$, while for the WD distribution $r_s \sim 0.5307$ [49]. Finite-size scaling assumes that for $\gamma > 2$ the value of r_s approaches the Poisson value as the matrix size grows, while for $\gamma < 2$, r approaches the WD value. At the transition ($\gamma = 2$) r should be independent of the matrix size. Thus, as one plots $r_s(\gamma)$ for larger values of N , the curve becomes more steplike, and all the curves are expected to cross at the same point. This has been seen in Ref. [37] and is reproduced here for larger matrix sizes. In Fig. 1(a) we plot $r(\gamma)$ for $N = 500, 1000, 2000, 4000, 16000, 48000$ with 12800, 6400, 3200, 1600, 800, 100 different matrices. The curves can be scaled using $\tilde{\gamma} = |\gamma - \gamma_c|(N/N_0)^\beta$, with $\beta = 0.12$ and $\gamma_c = 2$, and $N_0 = 500$ was chosen as the smallest matrix size. As can be seen in Fig. 1(b), this scaling works well.

Thus, for the low-energy scale one finds very clear evidence of the transition between localized states and extended ones at $\gamma = 2$.

On the other hand, the transition between the NEE phase and the truly extended phase anticipated to occur at $\gamma = 1$ leaves no signature in the ratio statistics. This is expected, as the small energy scale corresponds to long times, and since the states are extended at very long times in both the ergodic and NEE phases, small energy scales cannot resolve the difference. Thus, one should probe energy scales that are much larger than the mean level spacing.

Two statistical measures will be considered: the level number variance for a given energy window and applying the SVD to the spectrum [40–42].

The first is also known as the number variance [39]. Specifically, for an energy window of size E , the average number of levels $\langle n(E) \rangle$ and the variance $\langle \delta^2 n(E) \rangle = \langle [n(E) - \langle n(E) \rangle]^2 \rangle$ are calculated. For the WD distribution $\langle \delta^2 n(E) \rangle = 0.44 + (2/\pi^2) \ln[\langle n(E) \rangle]$, while for the Poisson distribution $\langle \delta^2 n(E) \rangle = \langle n(E) \rangle$. One may argue that for the NEE phase ($1 < \gamma < 2$) one should expect $\langle \delta^2 n(E) \rangle = \chi \langle n(E) \rangle$, where $\chi = \gamma - 1$ [38,50].

A major concern for the variance method is that it relies on unfolding the spectrum. For rather smooth spectra, the details of unfolding and averaging over realizations should not affect the results, but for the NEE phase, where a nonsmooth spectral density is expected [17,30,38], the unfolding procedure might strongly influence results. A different way to study the properties of an ensemble of spectra originating from different realizations was recently suggested [40–42] based on tech-

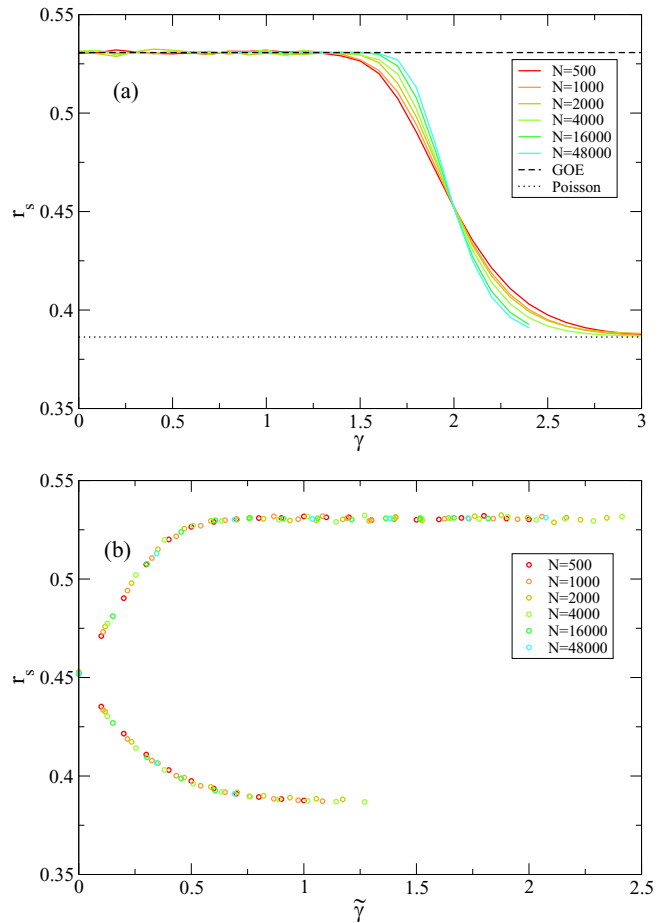


FIG. 1. The nearest neighbor level spacing statistics as manifested in the behavior of the ratio statistics $r(\gamma)$ for different values of γ and matrix size N . (a) The finite-size dependence of $r_s(\gamma)$. All curves cross at the critical value $\gamma_c = 2$ and exchange their order as they cross this point. This is a clear manifestation of a second-order phase transition. (b) Finite-size scaling. All curves neatly fall on the two branches above and below the transition as a function of $\tilde{\gamma}$ defined in the text.

niques originating in signal analysis. Given L realizations of P eigenvalues each, one defines a matrix X of size $L \times P$, where X_{lp} is the p level of the l th realization. X is SVD decomposed as $X = U \Sigma V^T$, where U and V are $L \times L$ and $P \times P$ matrices, respectively, and Σ is a diagonal matrix of size $L \times P$ and rank $r = \min(L, P)$. The r diagonal elements of Σ , denoted as σ_k , are the singular values of X and may be ordered such that $\sigma_1 \geq \sigma_2 \geq \dots \geq \sigma_r$. Essentially, this is a nonperiodic mode decomposition of the series. Defining $\lambda_k = \sigma_k^2$ represents the fraction of the total variance in the series captured by the mode. The lower singular values capture the global trends of the spectra, while the higher values represent the local fluctuations. It has been postulated that for the higher values in the localized regime $\lambda_k \sim k^{-2}$, while in the extended regime $\lambda_k \sim k^{-1}$ [41,42], corresponding to $1/f$ noise behavior [51].

We have calculated $\langle \delta^2 n(E) \rangle$ for large matrices of size $N = 16000, 24000, 32000, 48000$ and 800, 200, 100, and 100 different realizations, respectively. For each realization N eigenvalues ϵ_i were obtained. The spectrum was then unfolded

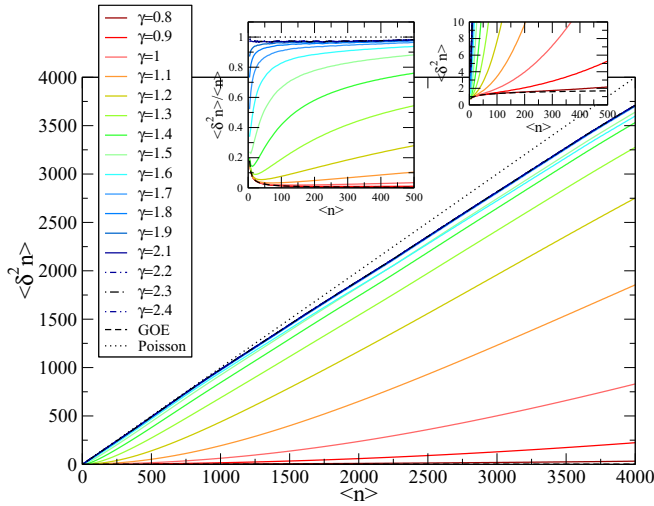


FIG. 2. The variance $\langle \delta^2 n(E) \rangle$ as a function of $\langle n(E) \rangle$ for the largest matrix size $N = 48000$ and values of γ between 0.8 and 2.4. The Poissonian and Wigner-Dyson behaviors are indicated. The top right inset zooms into the logarithmic behavior region, where deviations from the Wigner-Dyson behavior are seen even deep in the extended ergodic regime $\gamma < 1$. In the middle inset the variance normalized by n is plotted. Even in the localized regime $\gamma > 2$ some deviation from the Poisson value of 1 is seen.

by $\varepsilon_i = \varepsilon_{i-1} + 2m(\varepsilon_i - \varepsilon_{i-1}) / \langle \varepsilon_{i+m} - \varepsilon_{i-m} \rangle$, where $\langle \dots \rangle$ is an average over realizations and $m = 6$ (other values were used with no significant change). The center of the energy window is set at $E(j) = N/2 + j \times 20$, where for each realization $j = -j_{\max}, \dots, j_{\max}$ (with $j_{\max} = 150, 225, 300, 450$, i.e., the center of the energy window is located within a range of $3/16$ of the spectra around the middle). For each $E(j)$, the number of states in a window of width E centered at $E(j)$, $n_j(E)$, is evaluated; then the averages $\langle n(E) \rangle$ and $\langle n^2(E) \rangle$ are taken over all positions of the center j and realizations.

The variance $\langle \delta^2 n(E) \rangle$ as a function of $\langle n(E) \rangle$ is plotted in Fig. 2 for the largest matrix size, $N = 48000$, and different values of γ . Our main aim is to study the asymptotic behavior of the variance in large energy windows. Clearly, as γ increases, the variance switches from a Wigner-Dyson-like behavior to a Poisson-like behavior. Nevertheless, the observed behavior raises serious doubts about our ability to give definite answers on the asymptotic behavior from such data. Several factors compound the problem. It is clear that even for $\gamma < 1$ for which Wigner-Dyson behavior ($\langle \delta^2 n(E) \rangle = (2/\pi^2) \ln[\langle n(E) \rangle] + 0.44$) is expected, this behavior is followed up to only a certain n_{Th} , above which a stronger than linear dependence is seen. This scale n_{Th} depends both on γ (see the right inset in Fig. 2) and on the size of the matrix [see Fig. 3(a)]. This is similar to the deviation seen for the Anderson model [13,14,52] and in the SYK model [30] and is an indication of an energy scale known as the Thouless energy, $E_{\text{Th}} = \delta n_{\text{Th}}$, related to a timescale $t_{\text{Th}} = \hbar/E_{\text{Th}}$, indicating the typical time necessary to explore the system's available phase space. n_{Th} grows as the system becomes less sparse (lower γ) or larger in size.

As can be seen in Fig. 2 for $\gamma > 2$ and for different sizes in Fig. 3(b), deep in the Poisson regime ($\gamma > 2$), the expected

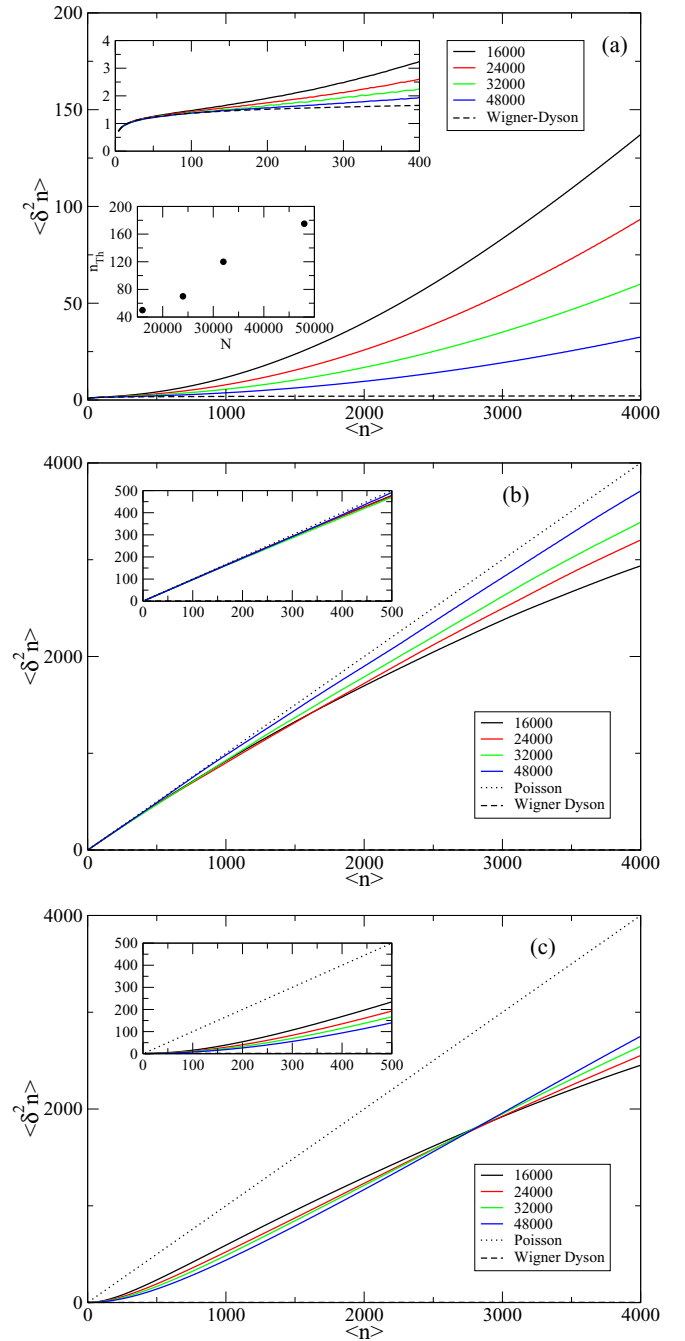


FIG. 3. The variance $\langle \delta^2 n(E) \rangle$ as a function of $\langle n(E) \rangle$ for (a) $\gamma = 0.8$ (WD regime), (b) $\gamma = 2.4$ (Poisson regime), and (c) $\gamma = 1.2$ (NEE regime) and matrix sizes between $N = 16000$ and $N = 48000$. A zoom into smaller values of n is shown in the insets. (a) Deep in the WD regime, it is clear that at n_{Th} deviations from the WD behavior are seen. The dependence of n_{Th} on size is presented in the bottom inset in (a). Above n_{Th} the variance grows stronger than linear and depends on N . (b) Deep in the Poisson regime. Up to $n \sim 500$ the behavior is linear, as expected from the Poisson regime. For higher n deviations to weaker dependence are seen. For larger systems the deviation appears for larger values of n . (c) In the NNE regime, the behavior deviates from WD almost immediately and follows a stronger than linear behavior, up to a point where a weaker dependence on n is seen.

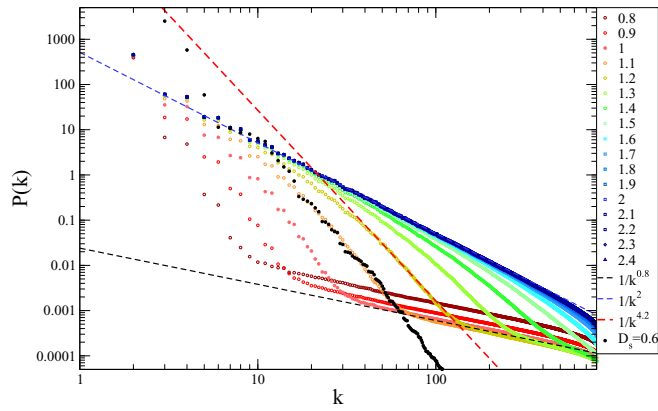


FIG. 4. The scree plots of ordered partial variances λ_k for 800 realizations of matrix size $N = 16000$ and different values of γ between 0.8 and 2.4. The expected behaviors for Poisson ($1/k^2$) and WD ($1/k^{0.8}$) and the transient behavior at $\gamma = 1.2$ ($1/k^{4.2}$) are indicated by dashed lines. A random Cantor set of spectra of $N = 4000$ and 1000 realizations with $D_s = 0.6$ (see text) corresponds to the solid black circles.

Poissonian behavior [$\langle \delta^2 n(E) \rangle = \langle n(E) \rangle$] is seen up to some value of n ($n \sim 1000$ for $N = 48000$ and $n \sim 500$ for $N = 16000$). Above this value $\langle \delta^2 n(E) \rangle$ grows weaker than linear. One could speculate that these deviations are a result of a combination of finite-size effects and the unfolding, which becomes less reliable at larger scales.

For the intermediate values of $1 < \gamma < 2$, where the NEE regime is expected, the behavior is even messier [Figs. 2 and 3(c)]. Almost immediately, the variance starts growing much faster than linear. As n increases, the growth peters out. One might fit a linear behavior with a slope smaller than 1, corresponding to the expected $\langle \delta^2 n(E) \rangle = \chi \langle n(E) \rangle$ behavior. Nevertheless, larger values of n remain strongly dependent on the size of the matrix [Fig. 3(c)] [53]. Thus, it is difficult to tease out the behavior at large n without *ad hoc* assumptions on the range of the fit.

Due to these difficulties, we switch to the SVD method, which does not require unfolding or calculation of the number variance. The scree plots of the ordered partial variances λ_k for 800 realizations of matrix size $N = 16000$ and $0.8 < \gamma < 2.4$ are presented in Fig. 4. Large k corresponds to small energy scales. Large energy scales depend on the overall density of states, which is not universal, and therefore, no information can be gleaned from $k \sim 1$. For the Poisson regime ($\gamma \geq 2$, indicated by purple symbols) $\lambda_{k>2}$ follows the expected k^{-2} behavior [41,42], up to deviations for large values of $k > 500$. In the WD regime ($\gamma \leq 1$, indicated by reddish symbols), for $k \geq 10$, λ_k follows k^α , with a slope $\alpha \sim 0.8$ —different from the expected slope $\alpha = 1$. As discussed in the Appendix, this is the effect of a finite number of realizations, much smaller than the number of eigenvalues ($L \ll P$). So for small energy scales, the WD behavior is followed up to an energy scale, which may be identified as E_{th} (corresponding to a value k_{Th}), above which a much steeper descent of $\lambda_{k < k_{\text{Th}}}$ is observed. This is in line with the number variance behavior.

The NEE regime ($1 < \gamma < 2$) shows intermediate behavior between WD behavior at large k and Poissonian behavior at

small values of k . This general behavior is expected since, as can be deduced from Fig. 3(c), at very short energy scales WD behavior is expected. At values of $\gamma > 1.6$ strong deviations from Poissonian behavior are seen at large values of k , and for $\gamma < 1.6$ large values of k show clear correspondence with WD. The range of energies for which WD holds increases as γ decreases. For large energies (small k), the complementary behavior is evident: Poissonian behavior is followed, whereas for larger γ the Poisson curve is joined earlier. Thus, for large energies the spectra follow Poissonian behavior, in agreement with the expectations of Ref. [50].

The crossover between the WD and Poissonian behaviors at intermediate values of k is most pronounced for $1 < \gamma < 1.6$. It seems that for a significant range of k a definite slope is followed, with a slope larger than Poissonian (super-Poissonian), which depends on γ . This is demonstrated for $\gamma = 1.2$, where a fit to $1/k^{4.2}$ is drawn. It is evident that a good fit in the range $40 < k < 120$ is obtained. A super-Poissonian (or multifractal metal) behavior has its origin in clustering of eigenvalues related to the miniband structure [17,38] for which the correlations between levels belonging to the same cluster (miniband) are much stronger than between those the minibands. In Ref. [17] a random Cantor set model which mimics the expected behavior of these minibands was proposed. Level spacings Δ are drawn independently from a power-law distribution $P(\Delta > \Delta_0) \sim \Delta_0/\Delta^{1+D_s}$ (where Δ_0 is a constant and D_s is a measure of fractality of the spectrum). As can be seen in Fig. 4, a random Cantor set, drawn from 1000 realizations of 4000 levels each, with $D_s = 0.6$, follows quite strikingly the behavior of $\gamma = 1.1$ for intermediate values of k . Similarly, decreasing values of D_s fit increasing values of γ . This lends strong support to the notion of a fractal (miniband) structure of the spectrum of the NEE phase for intermediate energy scales.

As for the number variance, one may wonder how sensitive the SVD method is to finite-size effects. In Fig. 5, we examine the dependence of the scree plot slopes on matrix sizes $N = 8000, 16000, 24000, 48000$ with 1000, 800, 200, and 100 realizations for WD ($\gamma = 0.8$), Poisson ($\gamma = 2$), and the NEE ($\gamma = 1.2$) regimes. Since the value of λ_k depends on size, for comparison we multiplied the curves by a constant to shift them one on top of the other for the same γ . In all cases a similar behavior of λ_k is seen for all sizes. The same holds for changing the number of realizations. Of course, the maximum k is reduced, but the overall behavior remains, as can be seen from Fig. 5 for $N = 16000$ and $\gamma = 1.2$, with 800, 400, and 200 realizations.

Thus, singular-value decomposition reveals robust super-Poissonian behavior for intermediate energy scales of the NEE phase for the parameter range $1.6 < \gamma < 2$. For $1 < \gamma < 1.6$, it is hard to observe the super-Poissonian regime since it is pushed to smaller energy scales, i.e., larger k . Moreover, the absolute slope decreases, and thus, the deviation from WD is less pronounced. Studying this regime will require a much larger number of realizations than what is available for this study. Demonstration of super-Poissonian behavior of the SVD analysis of energy spectra of other systems which are expected to show NEE behavior, for example, the disordered Josephson junction array [17] and granular SYK matter [54], may turn out to be very illuminating.

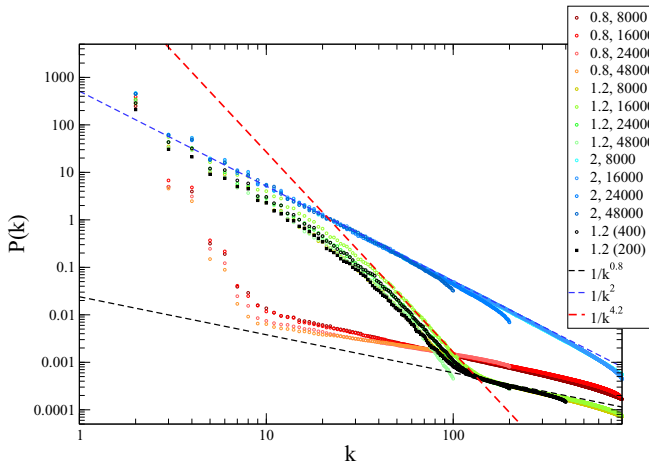


FIG. 5. The scree plots of ordered partial variances λ_k for different matrix sizes $N = 8000, 16000, 24000, 48000$ for 1000, 800, 200, and 100 realizations, respectively, and three different values of $\gamma = 0.8, 1.2, 2$. The curves for different matrix sizes were shifted by multiplying them by a constant so that they would overlap with the curves for $N = 16000$. The influence of the number of realizations is depicted by calculating λ_k for $N = 16000$, with only 400 and 200 realizations for $\gamma = 1.2$ (black symbols).

APPENDIX: SVD SCREE PLOT OF LARGE $1/f$ NOISE SERIES

By definition a $1/f$ noise series is a sequence with a power spectrum of $1/f$. Such a series may be numerically generated by different methods. Here we apply the method of Kasdin [55], using a recursive filter. We generate $L = 1600$ realizations with $P = 8192$ values each ($\{X_{p=1,L}^l\}$) and perform a discrete fast Fourier transform, $f^l(k) = (1/\sqrt{P}) \sum_p X_p^l \exp(-2\pi i k p/P)$, and then average the power spectrum over all realizations, $F(k) = \sum_l |f^l(k)|^2/L$. The modes are then ordered from $k = 1$ to $k = P$ and are shown in Fig. 6 as $F(k)$ vs k . The SVD of the matrix X is extracted. In SVD one essentially breaks matrix X into a sum of matrices (modes) each with their own amplitude (singular value) σ_k . After ranking $P(k) = \sigma_k^2$ from high to low ($k = 1$, highest amplitude) $P(k)$ vs k is plotted (known as a scree plot). As

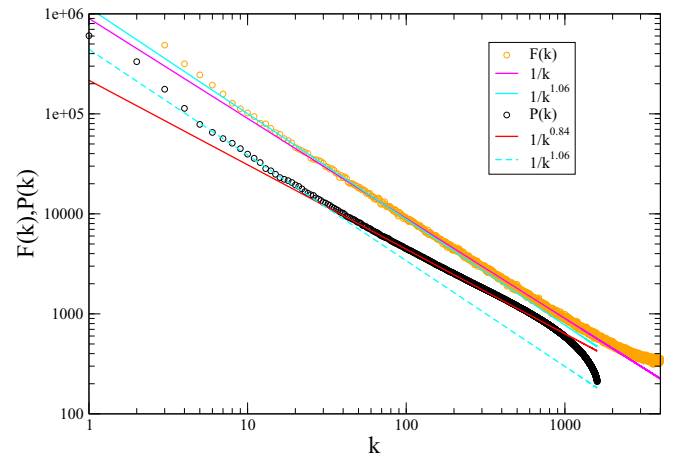


FIG. 6. Power spectrum $F(k)$ (orange circles) and scree plot of the SVD $P(k)$ (black circles) of an ensemble of numerically generated $1/f$ noise sequences of length 8192 for 1600 different realizations. Attempts to fit to different slopes are shown.

discussed in the main text, this plot has been shown to follow a distinct power-law behavior for the localized and extended phases, which makes it possible to identify the phases directly from the slope of the scree plot. In Fig. 6 we present the scree plot for $P(k)$ vs k .

The power spectrum shows the expected $1/k$ for the range $50 < k < 2000$. For $k < 50$, $F(k)$ takes a somewhat larger slope, $1/k^{1.06}$. The SVD scree plot is expected to follow the power spectrum slope [40–42,51]. Indeed, for $k < 50$, $P(k)$ follows with the same slope, $1/k^{1.06}$, while for $50 < k < 1000$, $P(k)$ corresponds to a different slope, $\sim 1/k^{0.84}$. It is important to note that while the Fourier transform results in $0 < k < P/2$ amplitudes and the number of realizations L determines only the quality of averaging, for the SVD one is limited to L eigenvalues. Therefore, if $P \ll L$, SVD will show a finite number of realization effects for a smaller value of k , resulting in the fact that although the Fourier transform shows a $1/k$ slope, the SVD results show a gentler slope. This trend is seen also in the main text, where although one expects the SVD in the WD regime to show a $1/k$ slope, it shows a slope closer to $\sim 1/k^{0.8}$.

[1] P. W. Anderson, *Phys. Rev.* **109**, 1492 (1958).
 [2] P. A. Lee and T. V. Ramakrishnan, *Rev. Mod. Phys.* **57**, 287 (1985).
 [3] B. Kramer and A. MacKinnon, *Rep. Prog. Phys.* **56**, 1469 (1993).
 [4] H. Aoki, *J. Phys. C* **16**, L205 (1983).
 [5] B. I. Shklovskii, B. Shapiro, B. R. Sears, P. Lambrianides, and H. B. Shore, *Phys. Rev. B* **47**, 11487 (1993).
 [6] T. Guhr, A. Muller-Groeling, and H. A. Weidenmuller, *Phys. Rep.* **299**, 190 (1998).
 [7] A. D. Mirlin, *Phys. Rep.* **326**, 259 (2000).
 [8] F. Evers and A. D. Mirlin, *Rev. Mod. Phys.* **80**, 1355 (2008).
 [9] V. E. Kravtsov, I. V. Lerner, B. L. Altshuler, and A. G. Aronov, *Phys. Rev. Lett.* **72**, 888 (1994).

[10] S. N. Evangelou, *Phys. Rev. B* **49**, 16805(R) (1994).
 [11] A. G. Aronov, V. E. Kravtsov, and I. V. Lerner, *Pis'ma Zh. Eksp. Teor. Fiz.* **59**, 40 (1994) [*JETP Lett.* **59**, 39 (1994)].
 [12] I. Kh. Zharekeshv and B. Kramer, *Phys. Rev. Lett.* **79**, 717 (1997).
 [13] B. Altshuler and B. Shklovskii, *Zh. Eksp. Teor. Fiz.* **91**, 220 (1986) [*Sov. Phys. JETP* **64**, 127 (1986)].
 [14] B. Altshuler, I. Zarekeshv, S. Kotochigova, and B. Shklovskii, *Zh. Eksp. Teor. Fiz.* **94**, 343 (1988) [*Sov. Phys. JETP* **67**, 625 (1988)].
 [15] A. G. Aronov and A. D. Mirlin, *Phys. Rev. B* **51**, 6131(R) (1995).
 [16] M. Pino, L. B. Ioffe, and B. L. Altshuler, *Proc. Natl. Acad. Sci. U.S.A.* **113**, 536 (2016).

- [17] M. Pino, V. E. Kravtsov, B. L. Altshuler, and L. B. Ioffe, *Phys. Rev. B* **96**, 214205 (2017).
- [18] T. Mithun, Y. Kati, C. Danieli, and S. Flach, *Phys. Rev. Lett.* **120**, 184101 (2018).
- [19] T. Mithun, C. Danieli, Y. Kati, and S. Flach, *Phys. Rev. Lett.* **122**, 054102 (2019).
- [20] E. J. Torres-Herrera and L. F. Santos, *Ann. Phys. (Berlin, Ger.)* **529**, 1600284 (2017).
- [21] R. Berkovits, *Ann. Phys. (Berlin, Ger.)* **529**, 1700042 (2017).
- [22] J. Lindinger, A. Buchleitner, and A. Rodríguez, *Phys. Rev. Lett.* **122**, 106603 (2019).
- [23] S. Roy, I. Khaymovich, A. Das, and R. Moessner, *Sci. Post Phys.* **4**, 025 (2018).
- [24] L. Faoro, M. Feigelman, and L. Ioffe, *Ann. Phys.* **409**, 167916 (2019).
- [25] K. Kechedzhi, V. Smelyanskiy, J. R. McClean, V. S. Denchev, M. Mohseni, S. Isakov, S. Boixo, B. Altshuler, and H. Neven [arXiv:1807.04792](https://arxiv.org/abs/1807.04792).
- [26] S. Sachdev and J. Ye, *Phys. Rev. Lett.* **70**, 3339 (1993).
- [27] J. Maldacena, *Int. J. Theor. Phys.* **38**, 1113 (1999).
- [28] J. Maldacena, S. H. Shenker, and D. Stanford, *J. High Energ. Phys.* **08** (2016) 106.
- [29] T. Micklitz, F. Monteiro, and A. Altland, *Phys. Rev. Lett.* **123**, 125701 (2019).
- [30] A. M. García-García and J. J. M. Verbaarschot, *Phys. Rev. D* **94**, 126010 (2016).
- [31] N. Rosenzweig and C. E. Porter, *Phys. Rev.* **120**, 1698 (1960).
- [32] V. E. Kravtsov, I. M. Khaymovich, E. Cuevas, and M. Amini, *New J. Phys.*, **17**, 122002 (2015).
- [33] C. Monthus, *J. Phys. A* **50**, 295101 (2017).
- [34] V. Kravtsov, B. Altshuler, and L. Ioffe, *Ann. Phys. (NY)* **389**, 148 (2018).
- [35] E. Bogomolny and M. Sieber, *Phys. Rev. E* **98**, 032139 (2018).
- [36] P. A. Nosov, I. M. Khaymovich, and V. E. Kravtsov, *Phys. Rev. B* **99**, 104203 (2019).
- [37] M. Pino, J. Tabanera, and P. Serna, *J. Phys. A: Math. Theor.* **52**, 475101 (2019).
- [38] G. de Tomasi, M. Amini, S. Bera, I. M. Khaymovich, and V. E. Kravtsov, *SciPost Phys.* **6**, 14 (2019).
- [39] M. L. Mehta, *Random Matrices*, 2nd ed. (Academic, New York, 1991).
- [40] R. Fossion, G. Torres Vargas, and J. C. López Vieyra, *Phys. Rev. E* **88**, 060902(R) (2013).
- [41] G. Torres-Vargas, R. Fossion, C. Tapia-Ignacio, and J. C. López-Vieyra, *Phys. Rev. E* **96**, 012110 (2017).
- [42] G. Torres-Vargas, J. A. Méndez-Bermúdez, J. C. López-Vieyra, and R. Fossion, *Phys. Rev. E* **98**, 022110 (2018).
- [43] E. Brezin and S. Hikami, *Nucl. Phys. B* **479**, 697 (1996).
- [44] T. Guhr, *Ann. Phys. (NY)* **250**, 145 (1996).
- [45] A. Altland, M. Janssen, and B. Shapiro, *Phys. Rev. E* **56**, 1471 (1997).
- [46] H. Kunz and B. Shapiro, *Phys. Rev. E* **58**, 400 (1998).
- [47] P. Shukla, *J. Phys.: Condens. Matter* **17**, 1653 (2005).
- [48] D. Facoetti, P. Vivo, and G. Biroli, *Europhys. Lett.* **115**, 47003 (2016).
- [49] Y. Y. Atas, E. Bogomolny, O. Giraud, and G. Roux, *Phys. Rev. Lett.* **110**, 084101 (2013).
- [50] V. E. Kravtsov and K. A. Muttalib, *Phys. Rev. Lett.* **79**, 1913 (1997).
- [51] A. Relaño, J. M. G. Gómez, R. A. Molina, J. Retamosa, and E. Faleiro, *Phys. Rev. Lett.* **89**, 244102 (2002).
- [52] D. Braun and G. Montambaux, *Phys. Rev. B* **52**, 13903 (1995).
- [53] S. Sadhukhan and P. Shukla, *Phys. Rev. E* **96**, 012109 (2017).
- [54] A. Altland, D. Bagrets, and A. Kamenev, *Phys. Rev. Lett.* **123**, 106601 (2019).
- [55] N. J. Kasdin, *Proc. IEEE* **83**, 802 (1995).